Mixed Metal Oxide Systems Applied to Thermochemical Storage of Solar Energy: Benefits of Secondary Metal Addition in Co and Mn Oxides and Contribution of Thermodynamics

Laurie Andre, Stéphane Abanades, Laurent Cassayre

applied sciences

MDPI

Article

Mixed Metal Oxide Systems Applied to Thermochemical Storage of Solar Energy: Benefits of Secondary Metal Addition in Co and Mn Oxides and Contribution of Thermodynamics

Laurie André [1], Stéphane Abanades [1,*] and Laurent Cassayre [2]

[1] Processes, Materials, and Solar Energy Laboratory, PROMES-CNRS, 7 Rue du Four Solaire, 66120 Font-Romeu, France; laurie.andre@promes.cnrs.fr

[2] Laboratoire de Génie Chimique, Université de Toulouse, CNRS, Toulouse, France; laurent.cassayre@ensiacet.fr

* Correspondence: stephane.abanades@promes.cnrs.fr; Tel.: +33-4-68-30-77-30

Received: 19 October 2018; Accepted: 8 December 2018; Published: 14 December 2018

Abstract: Thermochemical energy storage is promising for the long-term storage of solar energy via chemical bonds using reversible redox reactions. The development of thermally-stable and redox-active materials is needed, as single metal oxides (mainly Co and Mn oxides) show important shortcomings that may delay their large-scale implementation in solar power plants. Drawbacks associated with Co oxide concern chiefly cost and toxicity issues while Mn oxide suffers from slow oxidation kinetics and poor reversibility. Mixed metal oxide systems could alleviate the above-mentioned issues, thereby achieving improved materials characteristics. All binary oxide mixtures of the Mn-Co-Fe-Cu-O system are considered in this study, and their properties are evaluated by experimental measurements and/or thermodynamic calculations. The addition of Fe, Cu or Mn to cobalt oxide decreased both the oxygen storage capacity and energy storage density, thus adversely affecting the performance of Co_3O_4/CoO. Conversely, the addition of Fe, Co or Cu (with added amounts above 15, 40 and 30 mol%, respectively) improved the reversibility, re-oxidation rate and energy storage capacity of manganese oxide. Computational thermodynamics was applied to unravel the governing mechanisms and phase transitions responsible for the materials behavior, which represents a powerful tool for predicting the suitability of mixed oxide systems applied to thermochemical energy storage.

Keywords: concentrated solar energy; solar power; thermochemical energy storage; mixed metal oxide; redox reaction; computational thermodynamics

1. Introduction

The intermittent nature of solar energy used to drive concentrated solar power (CSP) plants calls for a suitable energy storage system, which will grant us the freedom to produce and dispatch electricity according to the population needs. Thermal energy storage (TES) can serve this purpose to match the variable electricity demand with the intermittent energy source supply, and much progress has been achieved with latent heat and sensible heat storage systems already in use in CSP plants [1–4]. Alongside these conventional modes of heat storage, thermochemical energy storage (TCES) is an attractive option to store solar energy at higher temperatures (400–1200 °C) and to be compatible with next generation CSP plants, such as pressurized air-based solar tower receivers for power generation via gas turbines. These high-temperature processes associated with thermodynamic power cycles will enable higher solar to electricity conversion efficiency. TCES offers higher energy storage densities and

possible heat storage at room temperature in the form of stable solid materials, due to energy storage in the form of chemical bonds, which then relates to long-term/seasonal storage. Its main application goal is still related to day/night operation of the power block in a CSP plant for continuous electricity generation. This technology is based on reversible solid-gas reactions, in which the heat transfer fluid is also the reactive gas of the reaction, and the energy required for the endothermic reaction is provided by CSP (Equation (1)). The reverse reaction (exothermic) can then release the stored energy to be delivered to the heat transfer fluid.

$$AB(s) + Heat\ (CSP) \leftrightharpoons A(s) + B(g) \quad (1)$$

Active research is ongoing for the development of suitable TCES systems and for their commercial implementation. In this endeavor however, additional research and development is required to achieve long-term cost-effective systems as a suitable way to implement TCES in solar power plants [5]. Recently, Bayon et al. (2018) [6] reported an interesting economical evaluation of 17 potential systems for TCES implementation in solar power plants. As a few systems are known to hold suitable properties (reversibility, high energy storage density, availability at low cost and non-toxicity) for TCES application (such as $Ca(OH)_2/CaO$, $Sr(OH)_2/SrO$ and $Ba(OH)_2/BaO$; carbonate looping with $CaCO_3/CaO$ and $SrCO_3/SrO$; redox with BaO_2/BaO), their implementation would also be cost competitive with molten salts in the near term [6].

Various systems can be considered, other than metal oxides [3,7]. For example, hydroxides, and especially calcium hydroxide [8–14] shows promising results for TCES. The systems based on carbonates are also relevant for TCES application. Calcium [15–18] and strontium carbonate [18,19] systems are promising but still require structure stabilization to hinder sintering at high reaction temperatures. In the specific case of single metal oxides, air can be used as heat transfer fluid (Equations (2) and (3)), which allows operating with an open-loop system.

$$MO_{(ox)} + Heat \rightarrow MO_{(red)} + \alpha\ O_2(g) \quad (2)$$

$$MO_{(red)} + \alpha\ O_2(g) \rightarrow MO_{(ox)} + Heat \quad (3)$$

In particular, Co_3O_4/CoO and Mn_2O_3/Mn_3O_4 are known to be the most promising redox systems, while CuO/Cu_2O also demonstrates suitable TCES properties [20–26].

The interest of Co_3O_4/CoO for TCES application comes from its fast reaction kinetics, complete reaction reversibility, high energy storage capacity and excellent cycling stability with a transition temperature suited for CSP application (892 °C, Table 1), and with a measured gravimetric energy storage density of 576 kJ/kg [27], while the theoretical reaction enthalpy is reported to be as high as 844 kJ/kg [28–30]. It has been studied in various forms to be implemented within CSP reactors as an energy storage unit. A numerical model was developed by Singh et al. (2017) [31] to simulate the heat and mass transfer, and chemical reaction involving a cobalt-based material inside a thermochemical storage system. The numerical model was validated as it was compared to the experimental reaction of Co_3O_4/CoO coated on a cordierite honeycomb structure inside a prototype reactor. The model could accurately predict the performance of the storage reactor during the charge/discharge steps. The performance of cobalt oxide in different shapes, such as powders, foams, pellets and honeycomb structures made from the oxide or coated, was studied. For example, the use of small-scale honeycomb structures was considered by Karagiannakis et al. (2016) [32] and cobalt-based honeycomb structures were tested in air between 700 °C and 1000 °C. The honeycomb made of pure Co_3O_4 suffered from deformation during redox cycling due to extensive swelling caused by Co_3O_4/CoO phase transitions. The addition of 10 wt% Al_2O_3 to Co_3O_4, to form a honeycomb structure made of a Co_3O_4-Al_2O_3 composite, proved to efficiently restrain extensive swelling of Co_3O_4/CoO after several redox cycles, but decreased the material storage efficiency over time, due to the formation of cobalt aluminate. The performance of cobalt oxide-based foams and honeycomb structures was also studied in the range

of 800–1000 °C and compared to Co_3O_4 powder [28]. The full reduction/oxidation of the total mass of Co_3O_4 coated on the supports (Al_2O_3, ZrO_2 and cordierite) was observed, as opposed to Co_3O_4 on SiC supports. Moreover, no detrimental interaction between the cobalt oxide and the support, such as Al_2O_3, ZrO_2 and cordierite, was reported. Furthermore, the protection of SiC with a SiO_2 layer also proved to offer a full conversion of the material.

Flow-through pellets, perforated monolithic bodies of Co_3O_4, or composites of Co_3O_4 with ceria, zirconia, alumina, iron oxide, silicon carbide and manganese oxide, were investigated by Pagkoura et al. (2014) [33] for energy storage applications in CSP plants. Based on their good heat storage capacity and thermo-mechanical stability, both cobalt oxide-alumina and cobalt oxide-iron oxide were considered very promising in this study. On the other hand, the addition of ceria (25 wt%) enhanced the reaction kinetics of cobalt oxide, while the corresponding pellets exhibited poor thermo-mechanical stability. A change in the temperature for the beginning of the reduction/oxidation reaction was also observed with a modification in the added second oxide.

The performance of commercial Co_3O_4 powder in a fixed bed with air flow was appraised in a vertical quartz tube heated between 765 °C and 930 °C: full conversion and very good cycling stability over eight successive cycles were observed. A comparable study was conducted with commercial Co_3O_4 shaped into porous foams placed within a ceramic tube heated by a horizontal furnace. Full conversion and good cyclability were again obtained. The material shaping neither affected the reactivity, nor the Co_3O_4 stability [34].

Nonetheless, cobalt oxide is a potentially carcinogenic material and is expensive [6], which gives incentives for the development of other alternative materials. The manganese oxide system (Mn_2O_3/Mn_3O_4) features slow kinetics of the oxidation step, which impacts the cycling reversibility of this material and requires performance improvement, but it is a less expensive raw material than cobalt oxide [35–37]. This system can achieve a gravimetric energy storage density of 110 to 160 kJ/kg [37,38] and the theoretical reaction enthalpy is reported to be 202 kJ/kg [37]. While Co_3O_4/CoO performs redox cycles with rapid reaction kinetics, Mn_3O_4 is very slow to re-oxidize and also presents a larger hysteresis than cobalt oxide [35–38]. Thus, the redox properties of Mn_2O_3/Mn_3O_4 need to be improved further to use this material efficiently for TCES application. A few works investigated the improvement of Mn_3O_4 re-oxidation kinetics via a change in morphology and shape of the initial material. The impact of the initial particle size on the cyclability of manganese oxide was studied [39], as well as the influence of the morphology and shape on the redox kinetics of the material [38,39]. The initial particle size influences the redox behavior of the metal oxide as smaller particles are more prone to material sintering and densification, which then hinders O_2 diffusion to the reacting core, then affecting the re-oxidation step [39,40]. In addition to the influence of initial particle size on the reaction kinetics, a sintering issue can also be encountered especially for smaller particles that favor material sintering [39]. Due to this fact, the material re-oxidation can be observed in two steps, first during the temperature cooling down of the discharge step, then continuing during the next heating up of the following charging step, although the re-oxidation is sometimes not observed at all [7,38,39]. The performance of Mn_2O_3 powders resulting from different synthesis methods (modified Pechini method and precipitation in ammonia [7,34]) was compared, along with data from commercial powder. The material synthesized by Pechini and commercial powder showed very low re-oxidation, while the reduced powder from the synthesis by precipitation in ammonia was re-oxidized up to 93%. Both synthetic powders were subjected to sintering, however the latter formed a porous structure described as "coral-like" [39] which allowed for oxygen circulating within the material.

As for the copper oxide (CuO/Cu_2O), it has been studied for air separation applications [23], but has also attracted attention for TCES application as it presents high energy storage capacity, 811 kJ/kg [21,25] and the reaction temperature is suitable to be used with CSP [21,22,25]. However, the melting point of copper oxide is very close to the transition temperature and sintering issues are increased, which is not convenient to achieve a good cycling stability [25]. The onset temperature for the reduction of copper oxide was measured around 1028 °C under 20% O_2/Ar (Table 1) during the

sample heating up [7]. The onset temperature measured for the re-oxidation during the next cooling down step was around 1002°C. The material showed a good reversibility, however not total, with a maximum conversion of 88% observed with temperature kept constant at 950 °C. In another TGA study in air, a re-oxidation of 92% for one cycle has been observed [23], with reduction and oxidation temperatures at 1075 °C and 1000 °C, respectively. The suitability of CuO/Cu_2O for TCES was also tested in a rotary kiln reactor [21], in which the material suffered from sintering and thus to loss in capacity, with incomplete reduction (80% in Ar, 40% in air) and low re-oxidation (~9%).

Lastly, the Fe_2O_3/Fe_3O_4 redox pair may also be a very attractive material for its low price and high availability. The Fe_2O_3/Fe_3O_4 redox pair also presents a high reaction enthalpy but the transition in air occurs at very high temperature (1392 °C [41]). The development of an efficient and suitable material for TCES application by incorporating iron oxide would help obtaining a more cost-effective energy storage medium with enhanced properties [6]. The reduction of Fe_2O_3 to Fe_3O_4 was observed under 20% O_2 atmosphere around 1391 °C (Table 1), and reduction at lower temperature can be achieved under inert atmosphere (958 °C in Ar). Fe_3O_4 was then capable to regain 92 wt% of the previously released oxygen. When studied in air, Fe_3O_4 could be re-oxidized up to 80% (750–900 °C), and a decrease in conversion rate was noticed and attributed to the formation of an oxidized impervious layer which became thicker with increasing temperature [42]. Iron-based materials offer high gravimetric energy storage density as iron is a widely available and cheap material. However, used as such, raw Fe_2O_3 is reduced at very high temperature and thus presents a high risk to encounter sintering.

Nowadays, the development of alternative TCES materials with suitable properties for long-term exploitation in CSP plants remains a challenge. Single-metal oxide systems can hardly compete with Co_3O_4/CoO in terms of energy storage density, reaction kinetics and cycling stability. It is possible to achieve better redox performance with a metal oxide by modifying its morphology (for example through tailored synthesis), or through the addition of a secondary transition metal. In previous works, this method has been applied to modify single metal oxides, chiefly Co_3O_4 and Mn_2O_3, and the impacts of this modification on the tuning of reaction kinetics, cycling stability and reaction temperature, were reported [34–36]. The present work aims to compare experimental assessment of mixed metal oxide systems based on Co_3O_4/CoO and Mn_2O_3/Mn_3O_4 through binary mixing between Co, Mn, Fe and Cu oxides to provide an overview of the most suitable systems and to propose perspectives for future development of oxide-based TCES technology. In addition, the contribution of thermodynamics is presented for the better understanding of the underlying mechanisms governing the redox chemistry of the binary oxide systems. It relies on existing phase diagrams and thermodynamic models of the ternary systems M-M'-O in air (where M and M' are two different metals from Co, Mn, Fe and Cu).

2. Materials and Methods

The redox activity of the synthesized mixed metal oxides was analyzed through simultaneous thermogravimetric analysis and differential scanning calorimetry (TGA/DSC, Netzsch, Selb, Germany). The materials, in the form of fine powders, were transferred to a ceramic crucible for thermal analysis. They were then heated (at 10 °C/min), under 20% O_2/Ar (10 NmL/min for O_2 and 40 NmL/min for Ar) or Ar (40 NmL/min), to perform the reduction step (endothermal), also called the heat charging step. Afterwards, the cycle was completed by cooling down the temperature (at 10°C/min) and performing the heat discharging step through the material re-oxidation (exothermal) to its original stoichiometry (using the same 20% O_2/Ar mixture), to confirm the reaction reversibility. The same procedure was then repeated in the next cycles (total of 3 cycles).

The oxygen storage capacity (OSC) of the material was measured, corresponding to the mass of oxygen lost and recovered during these two steps (in wt% of the total mass of metal oxide). The onset temperature for both steps was measured using Netzsch Proteus software tool. A difference in temperature between the reduction and re-oxidation was observed due to kinetic limitations and was depicted by the presence of a hysteresis phenomenon. This gap in temperature gains from being reduced, as it will then require less sensible energy to perform charge/discharge cycles if the variation

in temperature between the two steps is minimized. Thanks to the combined DSC, the heat flow absorbed and released by the sample was also recorded and quantified in kJ/kg (ΔH) via the linear integration of endothermic (charge) and exothermic (discharge) reaction peaks. Experimental data concerning oxygen storage capacity of redox materials, transition temperatures during redox process, and reaction enthalpies were averaged over the course of three successive reduction/oxidation cycles for each material.

The hereafter presented experimental data were obtained using metal oxides synthesized via a modified Pechini method [43] from the corresponding metal nitrates (>98% purity) mixed with citric acid and ethylene glycol (>99% purity) in aqueous solution. The solution was heated up until obtaining a viscous solution. The powders were then calcined in air at 200 °C for 2 h and at 750 °C for 4 h in order to eliminate the organics and residues of the synthesis, and to stabilize the structure. Crystalline phases were analyzed, before and after cycling, with X-ray diffraction (XRD) using a PANanalytical XPert Pro diffractometer, Malvern Panalytical, UK (CuKα radiation, λ = 0.15418 nm). Detailed synthesis method and specific properties analysis can be found in previous works [35,36]. Throughout the study, the amount of secondary metal (M') added to the main metal (M) is referred to as x(M') (content of M' in molar fraction), corresponding to the molar ratio on metal basis, n(M')/((n(M) + n(M')).

3. Experimental Assessment of Mixed Metal Oxide Systems for TCES

None of the test has led to a melting of any redox pairs in the single-metal oxide systems, and complete reduction was generally achieved. However, the re-oxidation rates were low for all compounds except cobalt oxide [7]. Since Co_3O_4/CoO and Mn_2O_3/Mn_3O_4 are the two most promising materials for TCES, the potential of Co and Mn-based mixed oxides was investigated through the addition of a secondary metal, for example with copper [36,41], iron [27,35,41,44], or with one another [36,45]. A summary of the experimental data obtained in the present work is provided in Table 1.

Table 1. Experimental data obtained for the investigated oxide systems (with 20% O_2 in Ar), comprising onset temperatures, chemical conversions and reaction enthalpy (B = Bixbyite, C = Corundum, S = Spinel, H = Hausmannite, M = Monoxide, D = Delafossite).

TCES System		Onset Temperature (°C)		Temperature Gap (°C)	Conversion (%)	Exp. Reaction Enthalpy (kJ/kg)	Phase Transition & Redox Couple
		Reduction	Oxidation				
Co_3O_4/CoO		909	843	66	95.6	597	**S** Co^{III} → **M** Co^{II}
Mn_2O_3/Mn_3O_4		944	772	172	19.2	148	**B** Mn^{III} → **H** Mn^{II}
CuO/Cu_2O		1028	1002	26	87.1	536	**CuO** Cu^{II} → **Cu_2O** Cu^{I}
Fe_2O_3/Fe_3O_4		1391	1350	41	86	183	**C** Fe^{III} → **S** Fe^{II}
Co-Cu-O x(Cu)	0.03	896	860	36	94.3	574	**S** Co^{III} → **M** Co^{II}
	0.1	867	845	22	97.4	570	
	0.2	864	824	40	97.3	520	
	0.25	863	820	43	99.7	503	
	0.3	864	813	51	97.5	436	
	0.4	864	816	48	93	327	
	0.6	861	818	43	98.8	351	
	0.8	867	813	54	93.4	212	
Co-Fe-O x(Fe)	0.05	921	848	73	84.4	454	**S** Co^{III} → **M** Co^{II}
	0.1	931	896	35	83.9	365	
	0.25	933	914	19	82.4	224	
	0.4	941	945	4	82.5	51	
Mn-Co-O x(Co)	0.5	989 (Ar)	-	-	64.2	133	**S** Co^{III} → **M** Co^{II}
	0.6	942 (Ar)	-	-	84.7	200	
	0.7	930	877	53	96.7	306	
	0.8	933	873	60	96.6	296	
	0.9	920	871	49	97.9	427	
	0.95	937	991	54	94.9	319	

Table 1. *Cont.*

TCES System		Onset Temperature (°C)		Temperature Gap (°C)	Conversion (%)	Exp. Reaction Enthalpy (kJ/kg)	Phase Transition & Redox Couple
		Reduction	Oxidation				
Mn-Cu-O x(Cu)	0.05	900	no re-ox.	-	21.2	126	***B*** Mn^{III} → ***H*** Mn^{II}
	0.1	877	no re-ox.	-	10.7	-	
	0.2	811	no re-ox.	-	1.6	-	
	0.3	976	1040	64	90.8	-	-
	0.4	960	969	9	96.9	-	***S*** Cu^{II} → ***D*** Cu^{I}
	0.5	962	886	76	88.2	-	
	0.8	954	1000	46	89.7	354	
Mn-Fe-O x(Fe)	0.1	990	774	216	31	168	***B*** Mn^{III} → ***H*** Mn^{II}
	0.15	981	870	111	99.1	171	
	0.2	980	860	120	98.2	194	***B*** Mn^{III} → ***S*** Mn^{II}
	0.3	984	866	118	94.1	195	
	0.4	998	903	95	95.3	189	
	0.5	1014	937	77	94.7	189	

3.1. Co-Fe-O Mixed Oxide System

The effects of the Fe incorporation to Co_3O_4 (initial phase: $(Fe_xCo_{1-x})_3O_4$) was studied for amounts of Fe up to x(Fe) = 0.4 (Figure 1), as there is no phase transition for this system below 1200 °C in air for x(Fe) > 0.6 [35], which is the upper limit usually admitted for TCES application. Compared to pure Co_3O_4, the studied compositions feature lesser oxygen storage capacity (OSC) with increasing iron content (Figure 1a), which is partly ascribed to an increasing proportion of spinel phase which is not converted into monoxide for 0.1 < x(Fe) < 0.6, and to the presence of residual oxygen storage in the monoxide phase introduced by the iron addition.

A linear correlation between the variations in oxygen mass loss/gain and the reaction enthalpy is evidenced in Figure 2. It is in accordance with the experimental data obtained for the reaction enthalpy of Co-Fe-O mixed oxides.

A decrease in reaction enthalpy was also observed with the increasing addition of Fe, from small amounts up to x(Fe) = 0.4 (51 kJ/kg, against 597 kJ/kg for pure Co_3O_4) (Figure 1b). Block et al. (2014) [27] previously described that the incorporation of iron to cobalt oxide may contribute to the Co_3O_4 stability when added in small amounts (10%), by enhancing the microstructural stability of cobalt oxide while retaining suitable reaction enthalpies, whereas larger amounts of added iron oxide gradually reduce the reaction enthalpy of the redox systems. In contrast, a minor loss in oxygen exchange capacity upon cycling was evidenced for lower Fe contents 0.05 < x(Fe) < 0.1 [35]. Concerning the Co-Fe-O system, the gravimetric energy storage density of the mixed oxides is lower than that of both pure cobalt oxide and iron oxide [27,35].

A noticeable decrease in the temperature gap between the reduction and oxidation reactions is also observed with the addition of Fe from x(Fe) = 0.1 to x(Fe) = 0.4 (Figure 1c), which is convenient to reduce the amount of energy required to switch between the charge and the discharge steps of the system. Overall, the transition temperature for both reduction and oxidation is increased with the addition of Fe to Co_3O_4.

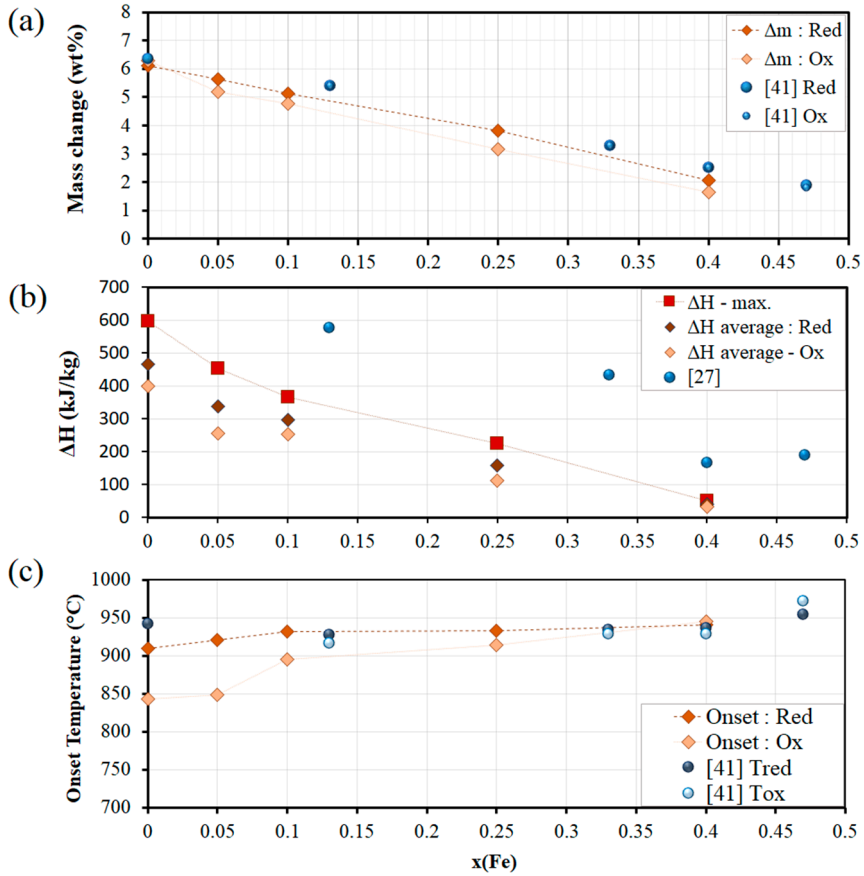

Figure 1. Mass variation (OSC), enthalpy change and onset temperatures of redox reactions measured for the Co-Fe-O system.

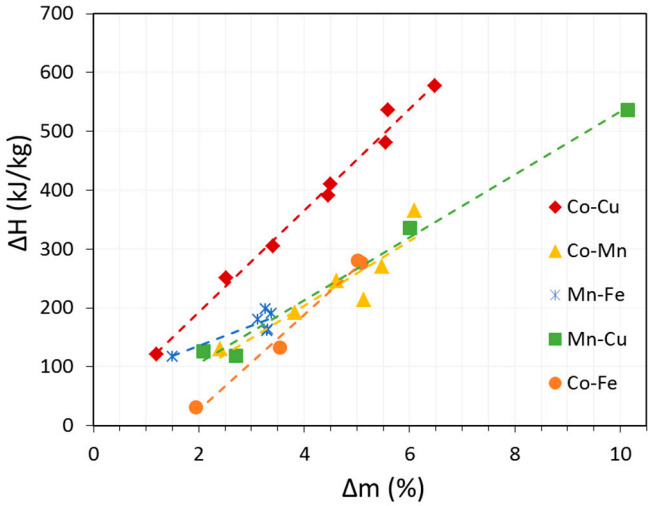

Figure 2. Correlation between measured enthalpy (average values from the reduction and oxidation reactions) and OSC (Δm) of Co-Fe, Co-Cu, Mn-Co, Mn-Fe and Mn-Cu mixed oxides.

3.2. Co-Cu-O Mixed Oxide System

The Co-Cu-O system shows very good reversibility and cycling stability for all the studied compositions up to x(Cu) = 0.8 [36,41] (Figure 3a). With higher copper content in the mixed oxide, the transition temperature of the system becomes too close to the melting point, thus increasing the presence of sintering issues with increasing copper amounts. However, this phenomenon did not alter

the reactivity of the materials. The OSC of this system also decreases, when compared to pure Co_3O_4, above x(Cu) = 0.03.

Similar to Co-Fe-O, a linear correlation was observed in the Co-Cu-O system between the OSC and the reaction enthalpy (Figure 2), since the decrease in OSC is accompanied by a linear decrease in the reaction enthalpy with increasing Cu amounts (Figure 3b). Depending on the composition, a lower enthalpy can be linked to a decrease in the reactive cobalt-containing phase, thus resulting in lower reaction enthalpies for compositions with higher copper amounts [41]. Motuzas et al. (2015) [46] studied the OSC of Co-Cu mixed oxides and also observed a favored oxygen exchange with higher cobalt content ($Co_{0.8}Cu_{0.2}O_x$), while the presence of copper oxide helped decreasing the temperature for the release of oxygen in cobalt oxide. The presence of non-reactive CuO for compositions around x(Cu) = 0.1 was also reported to stabilize the microstructure of the material against sintering [41].

Nonetheless, the reaction enthalpy of the Co-Cu-O system remains above 200 kJ/kg regardless of the Cu content, thus exhibiting high enough energy storage capacity to be of interest for TCES.

A noteworthy variation in reaction temperature occurs in the Co-Cu-O system since, on the one hand, the gap in temperature between reduction and oxidation decreases for x(Cu) < 0.1 (Figure 3c). On the other hand, the temperature difference is similar to that of the pure Co_3O_4 system for 0.1 < x(Cu) < 0.8 but both reduction and oxidation temperatures are shifted to lower values, thus providing an additional option to adapt the storage system to lower temperature conditions for energy storage application.

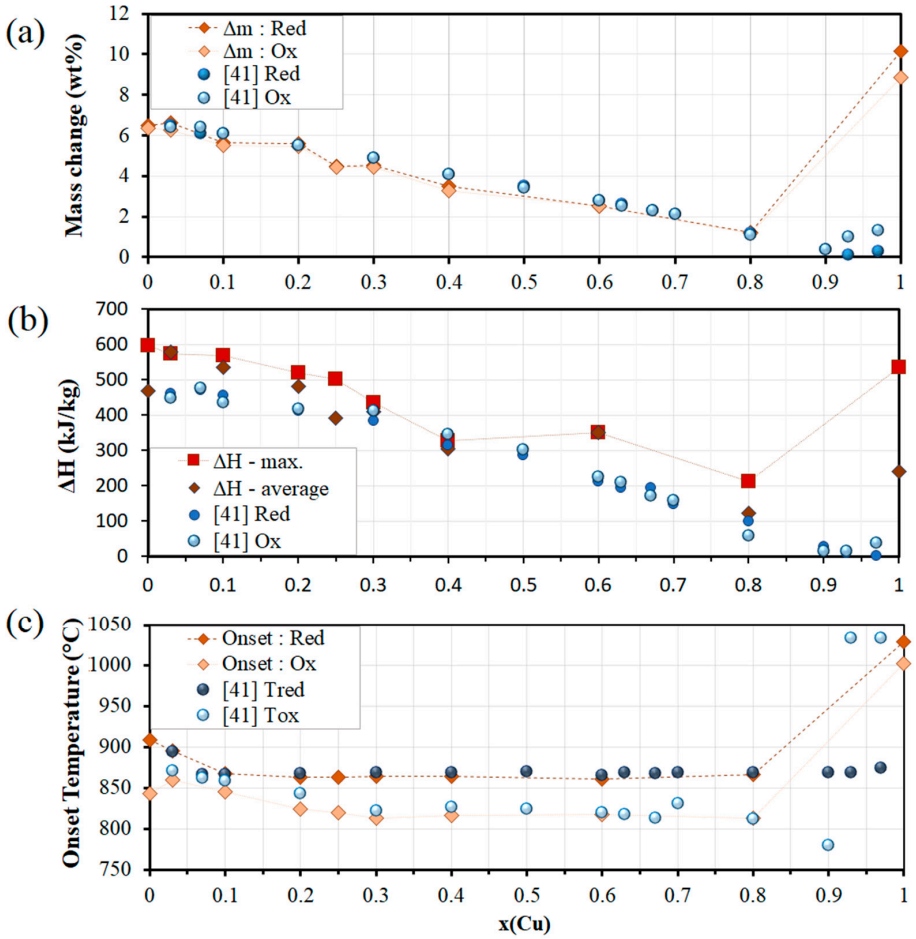

Figure 3. Mass variation (OSC), enthalpy change and onset temperatures of redox reactions measured for the Co-Cu-O system.

3.3. Mn-Fe-O Mixed Oxide System

The cycling stability and reversibility of the redox reaction of Mn_2O_3/Mn_3O_4 was greatly improved by the incorporation of iron from x(Fe) = 0.15 to x(Fe) = 0.5 (Figure 4a). This improvement concerning compositions above x(Fe) = 0.15 was attributed to the transition into a cubic spinel phase with increased re-oxidation capability, whereas for smaller Fe content the presence of the tetragonal spinel phase (hausmannite) is responsible for the poor re-oxidation [35,47]. Very good cycling stability was also reported in other studies with the incorporation of Fe contents higher than x(Fe) = 0.15 in manganese oxide. The mixed oxide with the composition $(Mn_{0.8}Fe_{0.2})_2O_3/(Mn_{0.8}Fe_{0.2})_3O_4$ has shown good stability over 75 redox cycles due to the incorporation of Fe modifying the structure and enhancing the oxidation rate [44]. The mixed oxide composition $(Mn_{0.75}Fe_{0.25})_2O_3$ also showed cycling stability and reversibility over the course of a hundred redox cycles, although a change in the particles' morphology was noted [47].

Concerning the overall OSC of the material, there was no change and it remained similar to that of pure Mn_2O_3 and stable for all the studied compositions (Figure 4a).

The reaction enthalpy also remained somewhat similar for all the studied compositions ($0 \leq$ x(Fe) ≤ 0.5), with a slight increase noticeable for x(Fe) = 0.2 (Figure 4b). However, when compared with the reaction enthalpies measured by Carrillo et al. (2015), it is difficult to conclude on a clear variation in the reaction enthalpy for compositions between $0 <$ x(Fe) < 0.2. Block et al. (2016) reported a measured enthalpy up to 232.7 kJ/kg for x(Fe) = 0.33 [41].

The temperature hysteresis of the Mn_2O_3/Mn_3O_4 system is a concern which could be addressed with the Fe addition in an amount superior to x(Fe) = 0.15, from which a clear decrease in the temperature gap is evidenced between the reduction and the oxidation temperatures (Figure 4c).

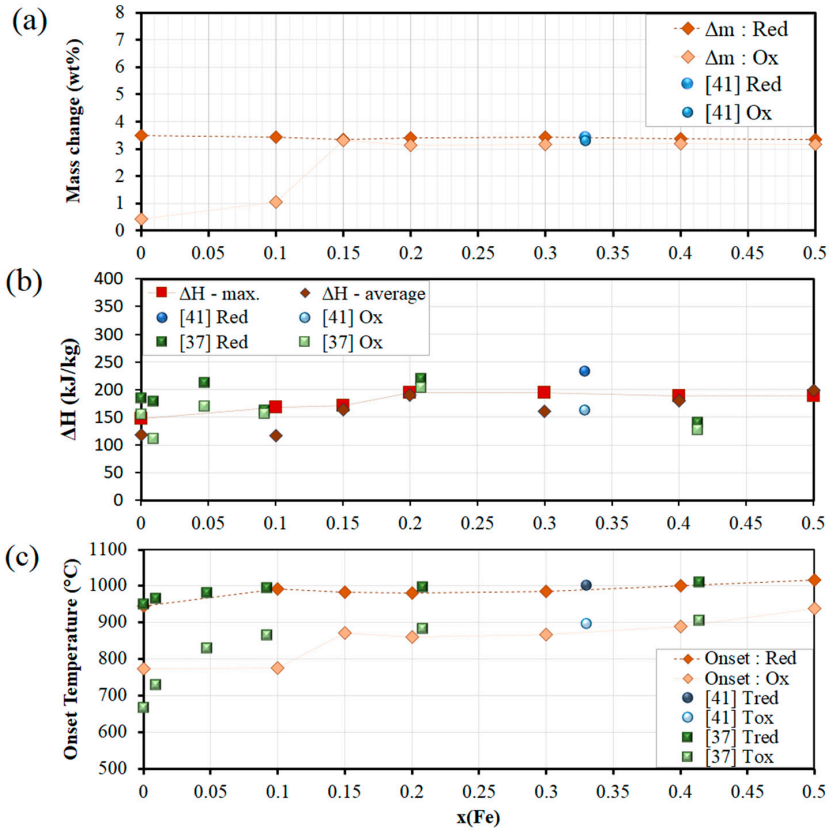

Figure 4. Mass variation (OSC), enthalpy change and onset temperatures of redox reactions measured for the Mn-Fe-O system.

3.4. Mn-Cu-O Mixed Oxide System

Within the Mn-Cu-O system, the reaction reversibility is poor for the compositions ranging from $0 \leq x(Cu) \leq 0.3$ (Figure 5a), as the material transitions through the hausmannite phase during the reduction step, with low re-oxidation capability [36], as also previously observed for Mn-based systems [35,36]. The hausmannite phase can be avoided completely by choosing a composition within the range $0.4 \leq x(Cu) \leq 0.8$, for which a good cycling stability is then observed, along with an increased OSC when compared to pure Mn_2O_3. The oxygen exchange capacity of a Mn-Cu mixed oxide with 34 wt% CuO was also investigated in a fluidized bed reactor and in TGA, and results showed complete cyclability for 18 cycles over the course of 35 h (reduction in N_2/oxidation in 10 vol% O_2:N_2) [48]. The addition of copper to Mn_2O_3 thus improves the cyclability of the material for $x(Cu) > 0.3$, but the sintering issue remains at high temperature and increases with increasing amounts of added copper [36].

The energy storage capacity of the Mn-Cu-O mixed oxides was found equal (148 kJ/kg for $x(Cu) = 0.4$ and 0.5) or higher (354 kJ/kg for $x(Cu) = 0.8$) than that of pure Mn_2O_3 for compositions with $x(Cu) > 0.4$ (Figure 5b). In order to avoid sintering and to keep the cost of the material at a minimum, mixed oxides of Mn-Cu-O with low copper amounts are preferred [36,41]. Block et al. (2016) [41] suggest that the composition at $x(Cu) = 0.5$ is also an option because of its melting point shifting from 1070 °C for the redox reaction of pure copper oxide to 1180 °C.

The reaction temperature is also modified by the addition of copper, as compositions with $x(Cu) \leq 0.3$ show lower reduction temperature than Mn_2O_3 (Figure 5c). The gap in temperature between oxidation and reduction is especially reduced for $x(Cu) = 0.4$ and $x(Cu) = 0.8$.

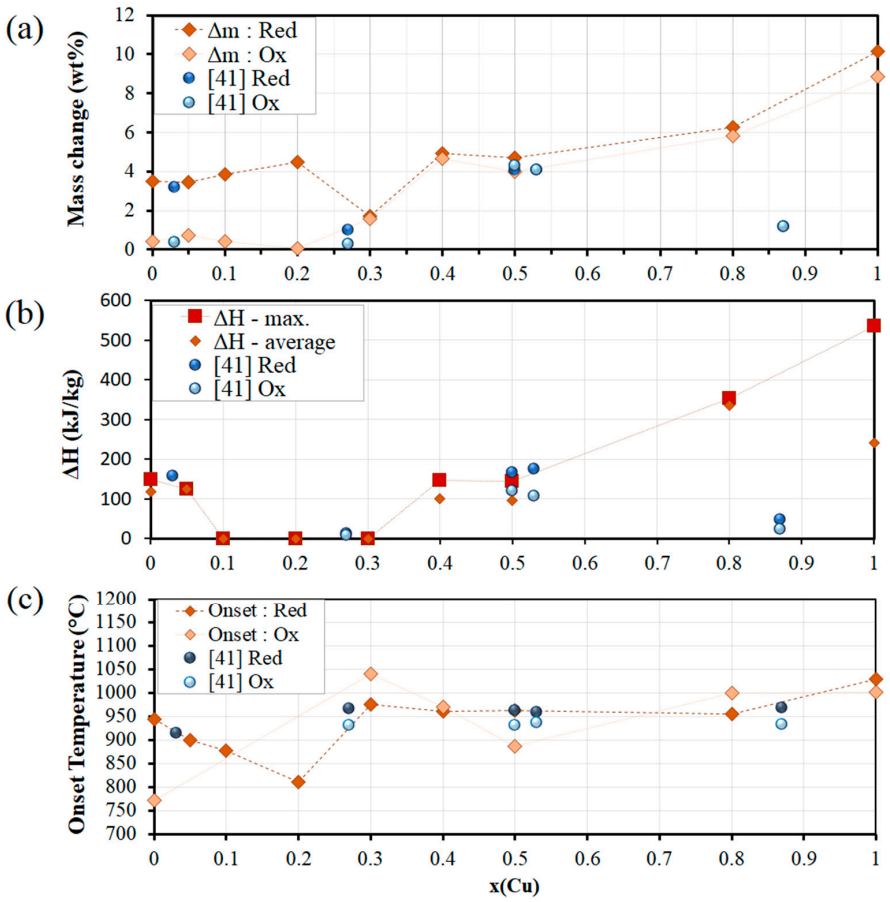

Figure 5. Mass variation (OSC), enthalpy change and onset temperatures of redox reactions measured for the Mn-Cu-O system.

3.5. Mn-Co-O Mixed Oxide System

In the Mn-Co-O system, the mixed oxides with higher Co content exhibit better reversibility (Figure 6a) and higher reaction enthalpy, while the OSC is decreased with increasing amounts of Mn added (Figure 6b) [36,41]. For compositions with x(Co) < 0.4, the low reaction reversibility and absence of re-oxidation is attributed again to the formation of the tetragonal spinel phase [36]. Nevertheless, the energy storage density remains higher for pure Co_3O_4 when compared to the mixed oxides within this system (Figure 6b), and the OSC and the reaction enthalpy follow a similar evolution (Figures 2 and 6a,b). However, the transition temperatures of the Mn-Co mixed oxides are higher than the transition temperatures of the pure cobalt oxide and manganese oxide (Figure 6c).

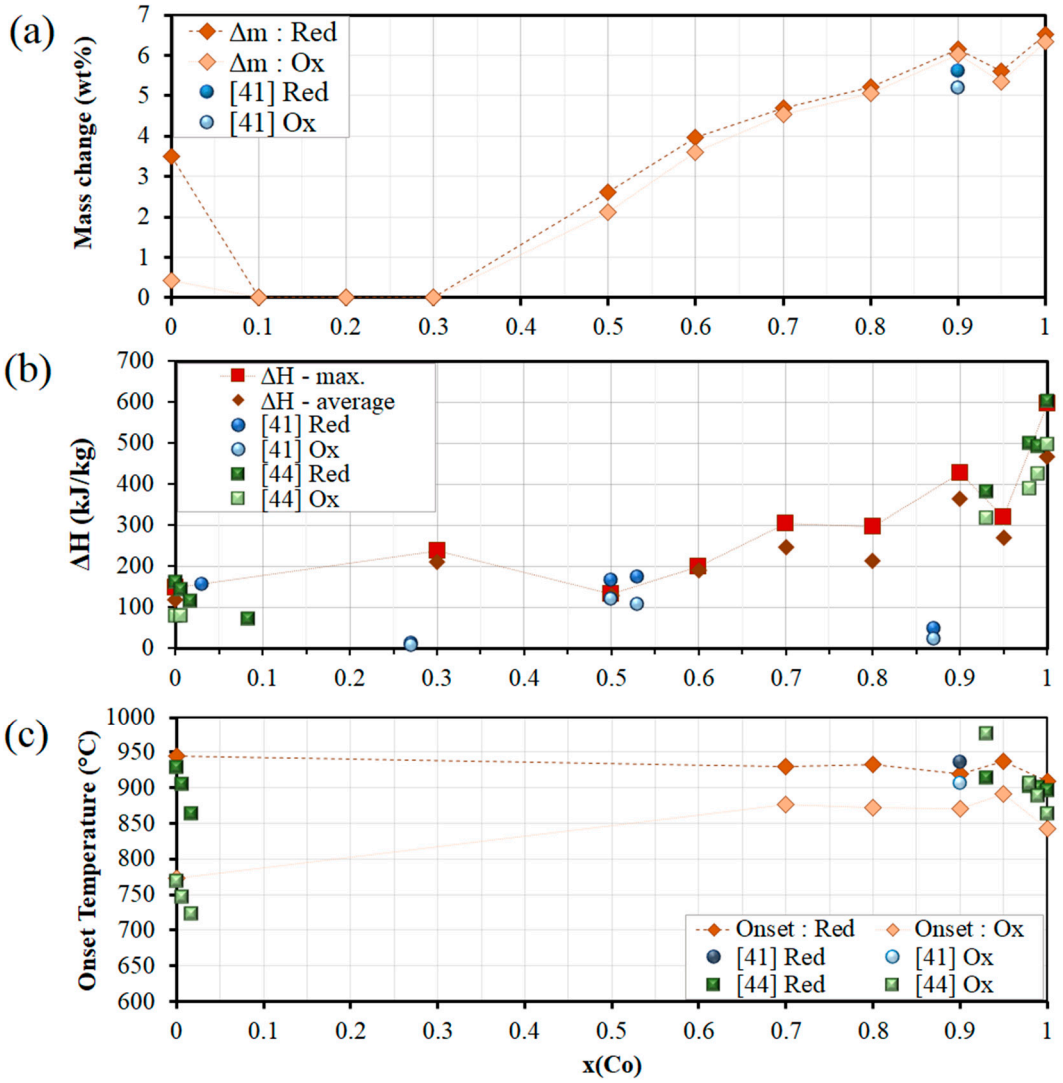

Figure 6. Mass variation (OSC), enthalpy change and onset temperatures of redox reactions measured for the Mn-Co-O system.

4. Contribution of Thermodynamic Calculations

Due to the implementation of high temperature chemical reactions in TCES processes, considerations related to thermodynamic equilibria are of high interest for the design of the most performant materials. Indeed, a precise thermodynamic description of the system $MM'O_{(ox)}$-$MM'O_{(red)}$-O_2(g) makes it possible to determine the maximum achievable conversion yield, to target the most suitable compositions and operating conditions, and to understand experimental results obtained at lab scale.

However, as illustrated by the case of the mixed oxides considered in this work, a full thermodynamic description of the systems is not always available. There are three major levels of thermodynamic description for such systems:

- Existence of an accurate phase diagram for the pseudo-binary system,
- Existence of thermochemical data such as enthalpy of mixing between phases or heat capacity functions ($c_{p(T)}$) for all phases of the system,
- Existence of a model established with the Calphad method, allowing equilibrium computations with a dedicated software.

When a full model is available, various equilibrium computations can be performed, such as the plot of phase diagrams or the calculation of the system equilibrium at various compositions and temperatures. This provides, for each composition and at each temperature step, the phase assemblage, the cationic distribution in each solution phases, the theoretical mass change (i.e., oxygen storage capacity), as well as the enthalpy variations of the system. As summarized in Table 2, three of the five systems considered here (Co-Fe-O, Co-Cu-O and Mn-Fe-O) benefit from a complete thermodynamic description including one or several models. However, this is not the case for the Mn-Co-O system, for which the phase diagram at temperatures below 800°C is not firmly established [49], nor for the Mn-Cu-O system, for which phase diagrams with large discrepancies have been published [50,51]. Among the global Mn-Co-Fe-Cu-O system, the last ternary sub-system, Cu-Fe-O, benefits from a large amount of experimental data and a robust model [52].

Table 2. Summary of available phase diagrams and thermodynamic models for the ternary systems Cu-Fe-O, Co-Fe-O, Co-Cu-O, Mn-Fe-O, Mn-Cu-O and Mn-Co-O in air [47–58].

Oxide System	Phase Diagram	Model
Cu-Fe-O	Jacob, 1977 [53]	Shishin, 2013 [52]
Co-Fe-O	Zhang, 2013 [54]	Jung, 2004 [55] Zhang, 2013 [54]
Co-Cu-O	Zabdyr, 2002 [56]	Zabdyr, 2002 [56]
Mn-Fe-O	Crum, 2009 [57]	Kjellqvist, 2010 [58] Kang, 2016 [47]
Mn-Co-O	Golikov, 1985 [49]	None
Mn-Cu-O	Driessens, 1967 [50] Wei, 2009 [51]	None

Depending on the level of description of the mixed oxide systems, several applications of thermodynamics are described in the following sections. The calculations were carried out with the FactSage software [59].

4.1. Hausmannite Phase Boundaries

One of the major conclusions of the experimental data compiled in Section 3, is that, for Mn-containing systems, the hausmannite phase formation has to be avoided, because of the poor reversibility of the phase transition during the cooling step of the thermal cycle. As illustrated with the three binary phase diagrams plotted in Figure 7, the binary systems based on Mn must contain a substantial amount (about 0.2 in molar fraction) of copper or iron oxide to make sure that the thermal cycle will not favor the appearance of the hausmannite phase at any temperature. In the case of cobalt additions, the hausmannite phase is stable on a much larger composition range.

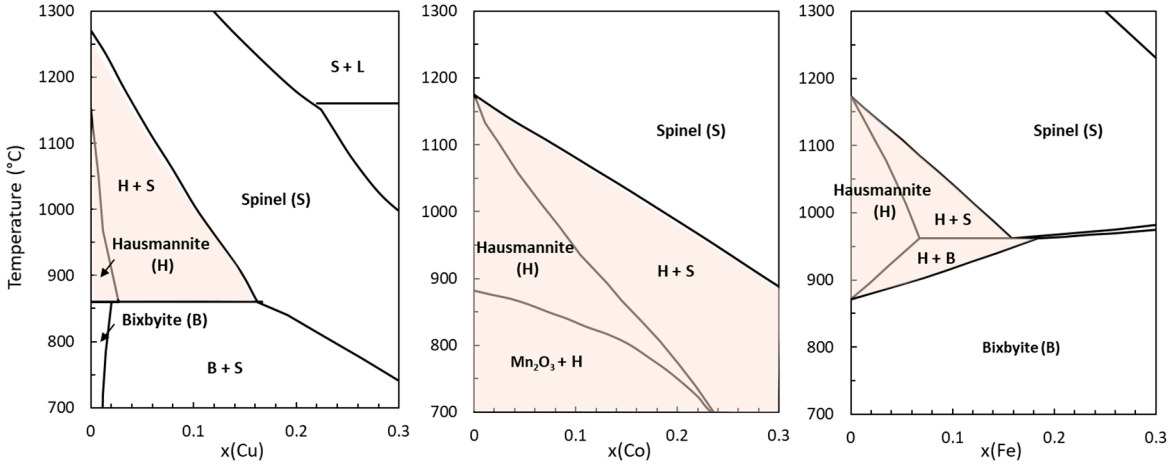

Figure 7. Mn-rich part of the Mn-Cu, Mn-Co and Mn-Fe phase diagrams in air (replotted from [49,51,57]).

The mixing of three metal oxides, rarely envisaged in TCES studies [60], can also be evaluated thanks to ternary phase diagrams. The only diagram of this type described in the literature is Mn-Co-Fe-O in air [61], for which the phase boundaries of Hausmannite at 800 and 1000 °C have been reproduced in Figure 8. This diagram shows that the combination of iron and cobalt additions does not significantly reduce the stability range of the hausmannite phase.

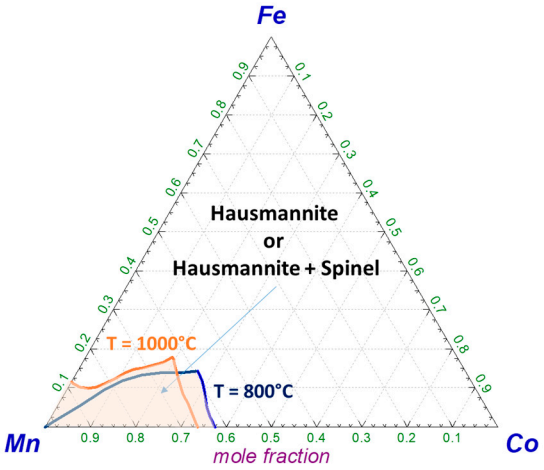

Figure 8. Composition domain containing the Hausmannite phase in the ternary system Mn-Co-Fe-O in air, at 800 and 1000 °C (from [61]).

Apart from the diagrammatic data discussed here, the use of a thermodynamic model is a strong support to explore a larger set of operation conditions. For instance, in the system Mn-Fe-O, equilibrium calculations show that the decrease of oxygen partial pressure in the gas phase is beneficial to the stability of the hausmannite phase (Figure 9). At low oxygen partial pressure, more Fe thus is required to stabilize the spinel phase.

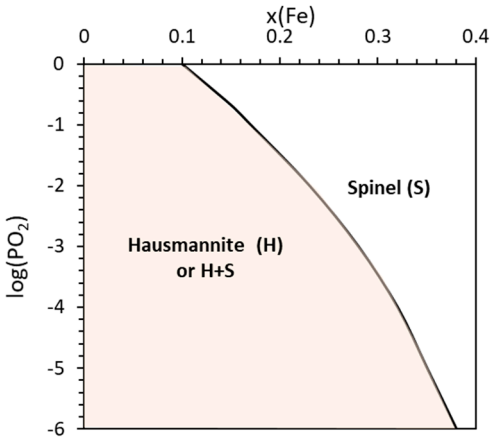

Figure 9. Calculated minimal amount of Fe in the Mn-Fe-O system in order to avoid the formation of the hausmannite phase at any temperature (model from [47]).

4.2. Phase Transitions in Mixed Oxide Systems

When dealing with solid-gas reactions involved in TCES processes, one must keep in mind a fundamental difference between single metal oxides and oxide mixtures. Indeed, according to the Gibbs' phase rule, the redox reactions (Equations (2) and (3)) for a single metal oxide occur at constant temperature. Conversely, with two metal oxides in the system, the variance increases, and the coexistence of two solid phases can occur on a large temperature and composition range.

A few typical examples of such behaviors are provided in Figure 10. The first case (Figure 10a,b) concerns the behavior of a single metal oxide, here Co_3O_4, with a phase transition occurring at 890 °C. Conversely, the phase transition between the spinel $(Co_{0.75}Fe_{0.25})O_4$ and the monoxide $Co_{0.75}Fe_{0.25}O$ (Figure 10c,d) occurs on a very large temperature range, between 935 and 1460 °C. However, most of the conversion of the spinel takes place in the first 100°C, and the enthalpy variation is also concentrated in this temperature range. This means that the maximal operating temperature does not need to be very high in order to store most of the achievable heat. Conversely, in the case of the conversion of the bixbyite $(Mn_{0.10}Fe_{0.90})_2O_3$ into the spinel $(Mn_{0.10}Fe_{0.90})_3O_4$ (Figure 10e,f), the concomitant formation of the hausmannite phase spreads the phase transition on about 200 °C, which implies a larger temperature of operation for the thermochemical cycle.

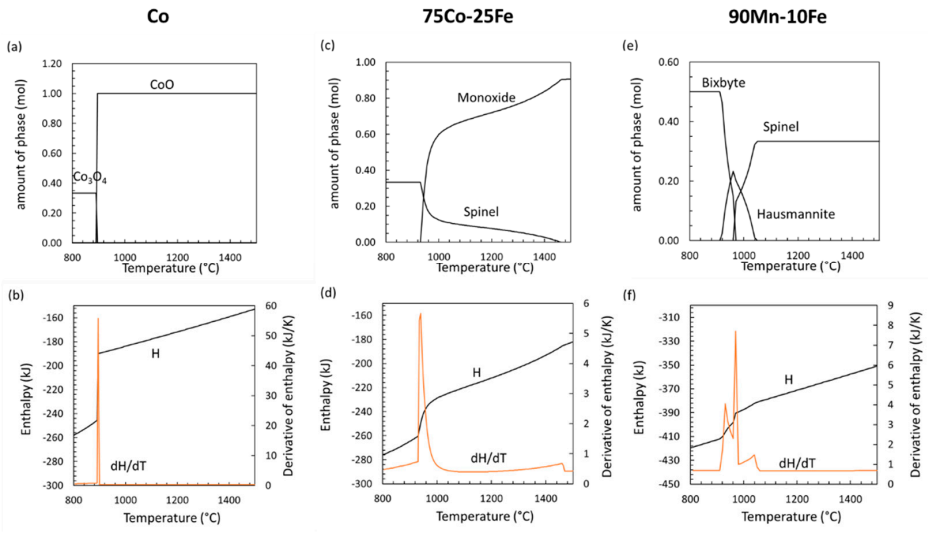

Figure 10. Calculation of the influence of temperature on (**a**,**c**,**e**) the phase assemblage evolution and (**b**,**d**,**f**) the system enthalpy, for three oxide systems in air.

4.3. Calculations in the Cu-Fe-O System

In the present work, no experimental measurements were carried out in the Cu-Fe-O system. However, the existence of a full thermodynamic model [52] makes it possible to evaluate the potentialities of such mixed oxides for the purpose of TCES applications.

As mentioned in Section 3, one of the main constraints regarding Cu-containing redox systems is to avoid the formation of a liquid phase. As shown by the phase diagram plotted in Figure 11a, some liquid phase forms at 1048 °C for 0 < x(Fe) < 0.50, due to the presence of an eutectic at x(Fe) = 0.15. Meanwhile, the minimal temperature to reach in order to reduce Cu^{II} into Cu^{I} is 1028 °C. Thus, in the composition range 0 < x(Fe) < 0.50, the addition of iron to copper oxide does not solve the problem of a very narrow window of operating temperature.

Figure 11b presents the mass variation (i.e., the OSC) in the whole Cu-Fe composition range, for various maximal cycle temperatures. In agreement with the two compositions studied by Block et al. (2016) [41], the calculations show that the addition of iron to copper oxide decreases the OSC if the maximal temperature is fixed at 1040 °C. For high iron content (x(Fe) > 0.66), the mass variation is very low. Indeed, in this case the TCES properties rely on the Fe^{III}/Fe^{II} redox reaction, which requires much higher temperatures (above 1200 °C). Figure 11b also clearly illustrates that a maximal temperature lower than 1040°C implies a low OSC for most of the Cu-Fe compositions.

Notably, the calculations evidence that the case of pure delafossite compound $CuFeO_2$ (x(Fe) = 0.5) may constitute the best compromise in the Cu-Fe-O systems. This stoichiometric compound allows for a higher maximal temperature of operation before decomposition (1075 °C instead of 1048 °C), with an OSC value of 4.9% as already confirmed by experimental studies devoted to delafossite properties [62], and a calculated transition enthalpy of 206 kJ/kg. This observation calls for a deeper investigation of the potentialities of $CuFeO_2$ for TCES applications.

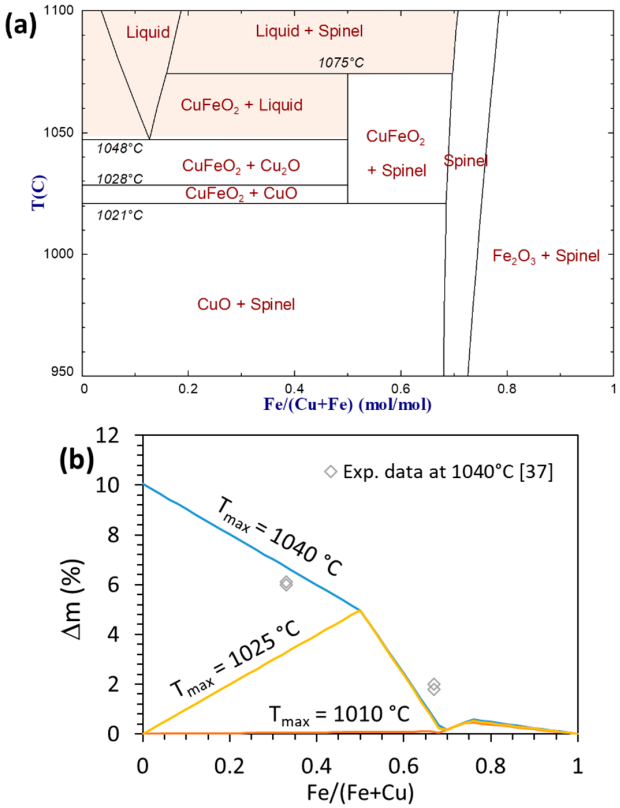

Figure 11. (**a**) Calculated phase diagram (model from [52]) of the Cu-Fe-O system in air, with highlight on the presence of the liquid phase (**b**) Evolution of mass change with composition for cycles between T_{min} = 800 °C and T_{max} = 1010, 1025 and 1040 °C.

5. Discussion and Conclusions

Thermochemical energy storage (TCES) is a promising route for the long-term storage of solar energy in the form of chemical bonds involving metal oxide systems. Indeed, the use of metal oxides for this application brings interesting alternative to other solid-gas systems because air can advantageously be used in open loop as both the reacting gas (O_2) in the reversible reactions and the heat transfer fluid (energy carrier from or to the storage medium). To cope with the noticeable challenges for developing reliable energy storage materials applied to solar power plants, binary and ternary metal oxide systems are considered. Their utilization could indeed alleviate the main critical issues related to singles oxides (cost and toxicity issues for Co oxide, poor reversibility due to slow oxidation rate for Mn oxide), and improved materials characteristics could be achieved such as resistance to sintering, compatible transition temperature, complete reaction reversibility, and suitable energy storage capacity.

Cobalt-based and manganese-based oxides have been investigated and compared with recent literature data in order to summarize the suitability of mixed oxides systems for TCES application at high temperature. The properties of mixed oxides regarding their energy storage capacity, redox reaction reversibility/cyclability, reaction temperature and hysteresis gap, were evaluated for the following systems: Co-Fe-O, Co-Cu-O, Mn-Fe-O, Mn-Cu-O and Mn-Co-O. Concerning cobalt-based systems, the addition of iron greatly decreases the OSC of the material, and the respective pure oxides show a higher reaction enthalpy than the mixed oxides of the Co-Fe-O system. However, the reaction temperature is positively impacted, as the hysteresis gap is reduced for compositions with $0.1 \leq x(Fe) \leq 0.4$. In addition, small amounts of added Fe, $x(Fe) \leq 0.1$, may contribute to the thermal stability of Co_3O_4. From these observations, the incorporation of Fe around x(Fe) = 0.1 might be relevant to obtain a TCES material with enhanced stability, lower temperature gap between reaction steps, still high enough energy storage density (even though lower than that of the pure Co oxide), slightly lower cost, and possible use for higher temperature application, when compared to pure Co_3O_4.

The mixed oxides investigated in the Co-Cu-O system retain high reaction enthalpy (over 200 kJ/kg) and show good stability over several redox cycles. Similar to the Co-Fe-O system, the reaction enthalpy reported for the Co-Cu mixed oxides decreases with increasing amounts of added Cu. The OSC of the mixed oxides follows the same trend, except for a very small Cu amount, x(Cu) = 0.03, for which the OSC is unchanged when compared to pure Co_3O_4. Furthermore, previous literature data attracted attention to low Cu-content compositions, especially around x(Cu) = 0.1, which was reported to hinder the material sintering, thus enhancing the stability of Co_3O_4 over repeated redox cycles, and improving its reaction kinetics. In addition, the addition of Cu to cobalt oxide reduces the transition temperature, thus providing a tunable option for storage systems requiring a different operating temperature.

The incorporation of Co into Mn_2O_3 contributed to the enhancement of the material properties, but both the OSC and energy storage capacity decrease with increasing amounts of Mn. The Mn-Co-O mixed oxides with a majority of cobalt in the composition might be an alternative, as these materials show good reaction reversibility and suitable reaction enthalpies. They could further reduce the cost of the storage system, as compared to pure Co_3O_4, taking into account that their performances are however by far lower than those of pure Co_3O_4.

Concerning the Mn-based system with Cu addition, compositions ranging from x(Cu) = 0.4 to x(Cu) = 0.8 show a good reversibility, higher OSC and similar reaction enthalpy than pure Mn_2O_3. The gap in temperature between the charge and discharge steps is especially reduced for x(Cu) = 0.4. When compared with literature data, the compositions with x(Cu) = 0.5 and x(Cu) = 0.8 also demonstrate suitable properties. Because higher Cu amounts imply increased effect of sintering and higher cost, the composition at x(Cu) = 0.8 should be thus avoided. From x(Cu) = 0.3, a good reaction reversibility is observed but a low OSC, whereas compositions with lower Cu content show low reaction reversibility due to the presence of the hausmannite phase. Similarly, the Fe addition shows a positive impact on Mn_2O_3 cycling activity. Reversibility and stability over redox cycles are achieved with Fe addition above x(Fe) = 0.15, while the OSC remains stable. The enthalpy also remains unchanged (around 190 kJ/kg for x(Fe) between 0.15 and 0.50). Besides, the temperature gap between

the reduction and oxidation is decreased with the addition of iron above x(Fe) = 0.15. The low material re-oxidation at low Fe content (x(Fe) < 0.15) comes from the formation of the tetragonal spinel phase (hausmannite). The hausmannite phase is no more stable when increasing the Fe content, and heating leads to a transition into a cubic spinel phase with enhanced re-oxidation capabilities.

In conclusion, the addition of iron to Co_3O_4 and Mn_2O_3 demonstrates the possible tuning of the systems temperatures to higher temperatures, while also reducing the hysteresis gap for both materials depending on the composition. The addition of Cu to Co_3O_4 also shifts the transition temperature to lower temperature. The Mn_2O_3 performance is greatly improved with the addition of a secondary metal in sufficient amounts to avoid the hausmannite phase formation during the heating. Although some compositions within Mn-Cu and Mn-Co systems are performant, Mn-Fe mixed oxides can exhibit high performance and be cost-effective due to the high availability of iron. Significant performance improvements can thus be achieved when considering mixed metal oxides and the limitations associated to both Co and Mn oxides (low re-oxidation yield, poor reversibility, large temperature gap between redox reactions, scarce availability and high cost) can be alleviated with secondary metal additives. The oxygen storage capacity and energy storage density stand out from a linear correlation that was unraveled for each type of binary oxide system, paving the way for the possible optimization of the heat storage capacity via the improvement of the oxygen exchange rates.

In addition, thermodynamic modelling and equilibrium calculations were shown to be a relevant support for predicting reliably the behavior of mixed oxide systems and phase transitions. The results provided consistent transition temperatures, oxygen storage capacities and enthalpies. The application of suitable models provided new physical insights into the role of secondary metal addition on the redox properties' improvement of Co and Mn-based oxides. The calculations also highlighted that the $CuFeO_2$ stoichiometric compound might be a relevant candidate material. The identification of new suitable mixed oxides could become possible with the development of new thermodynamic models encompassing large multi-component systems, which then would allow the selection of different transition metals for tuning the redox properties of mixed metal oxides for TCES applications.

Author Contributions: Data curation, S.A. and L.C.; Investigation, L.A., S.A. and L.C.; Supervision, S.A.; Writing—original draft, L.A.; Writing—review and editing, S.A. and L.C.

Funding: This research received no external funding.

Conflicts of Interest: The authors declare no conflict of interest.

References

1. Pardo, P.; Deydier, A.; Anxionnaz-Minvielle, Z.; Rougé, S.; Cabassud, M.; Cognet, P. A review on high temperature thermochemical heat energy storage. *Renew. Sustain. Energy Rev.* **2014**, *32*, 591–610. [CrossRef]
2. Yan, T.; Wang, R.Z.; Li, T.X.; Wang, L.W.; Fred, I.T. A review of promising candidate reactions for chemical heat storage. *Renew. Sustain. Energy Rev.* **2015**, *43*, 13–31. [CrossRef]
3. Abedin, A.H. A Critical Review of Thermochemical Energy Storage Systems. *Open Renew. Energy J.* **2011**, *4*, 42–46. [CrossRef]
4. Pelay, U.; Luo, L.; Fan, Y.; Stitou, D.; Rood, M. Thermal energy storage systems for concentrated solar power plants. *Renew. Sustain. Energy Rev.* **2017**, *79*, 82–100. [CrossRef]
5. Ströhle, S.; Haselbacher, A.; Jovanovic, Z.R.; Steinfeld, A. The effect of the gas-solid contacting pattern in a high-temperature thermochemical energy storage on the performance of a concentrated solar power plant. *Energy Environ. Sci.* **2016**, *9*, 1375–1389. [CrossRef]
6. Bayon, A.; Bader, R.; Jafarian, M.; Fedunik-Hofman, L.; Sun, Y.; Hinkley, J.; Miller, S.; Lipiński, W. Techno-economic assessment of solid-gas thermochemical energy storage systems for solar thermal power applications. *Energy* **2018**, *149*, 473–484. [CrossRef]
7. André, L.; Abanades, S.; Flamant, G. Screening of thermochemical systems based on solid-gas reversible reactions for high temperature solar thermal energy storage. *Renew. Sustain. Energy Rev.* **2016**, *64*, 703–715. [CrossRef]

8. Fujii, I.; Tsuchiya, K.; Higano, M.; Yamada, J. Studies of an energy storage system by use of the reversible chemical reaction: CaO + H_2O ⇌ $Ca(OH)_2$. *Sol. Energy* **1985**, *34*, 367–377. [CrossRef]
9. Pardo, P.; Anxionnaz-Minvielle, Z.; Rougé, S.; Cognet, P.; Cabassud, M. $Ca(OH)_2$/CaO reversible reaction in a fluidized bed reactor for thermochemical heat storage. *Sol. Energy* **2014**, *107*, 605–616. [CrossRef]
10. Linder, M.; Roßkopf, C.; Schmidt, M.; Wörner, A. Thermochemical energy storage in kW-scale based on CaO/$Ca(OH)_2$. *Energy Procedia* **2013**, *49*, 888–897. [CrossRef]
11. Dai, L.; Long, X.F.; Lou, B.; Wu, J. Thermal cycling stability of thermochemical energy storage system $Ca(OH)_2$/CaO. *Appl. Therm. Eng.* **2018**, *133*, 261–268. [CrossRef]
12. Criado, Y.A.; Huille, A.; Rougé, S.; Abanades, J.C. Experimental investigation and model validation of a CaO/$Ca(OH)_2$ fluidized bed reactor for thermochemical energy storage applications. *Chem. Eng. J.* **2017**, *313*, 1194–1205. [CrossRef]
13. Yan, J.; Zhao, C.Y. First-principle study of CaO/$Ca(OH)_2$ thermochemical energy storage system by Li or Mg cation doping. *Chem. Eng. Sci.* **2014**, *117*, 293–300. [CrossRef]
14. Criado, Y.A.; Alonso, M.; Abanades, J.C. Enhancement of a CaO/$Ca(OH)_2$ based material for thermochemical energy storage. *Sol. Energy* **2016**, *135*, 800–809. [CrossRef]
15. Ortiz, C.; Romano, M.C.; Valverde, J.M.; Binotti, M.; Chacartegui, R. Process integration of Calcium-Looping thermochemical energy storage system in concentrating solar power plants. *Energy* **2018**, *155*, 535–551. [CrossRef]
16. Chen, X.; Jin, X.; Liu, Z.; Ling, X.; Wang, Y. Experimental investigation on the CaO/$CaCO_3$ thermochemical energy storage with SiO_2 doping. *Energy* **2018**, *155*, 128–138. [CrossRef]
17. Benitez-Guerrero, M.; Valverde, J.M.; Sanchez-Jimenez, P.E.; Perejon, A.; Perez-Maqueda, L.A. Multicycle activity of natural $CaCO_3$ minerals for thermochemical energy storage in Concentrated Solar Power plants. *Sol. Energy* **2017**, *153*, 188–199. [CrossRef]
18. André, L.; Abanades, S. Evaluation and performances comparison of calcium, strontium and barium carbonates during calcination/carbonation reactions for solar thermochemical energy storage. *J. Energy Storage* **2017**, *13*, 193–205. [CrossRef]
19. Wu, S.; Zhou, C.; Doroodchi, E.; Nellore, R.; Moghtaderi, B. A review on high-temperature thermochemical energy storage based on metal oxides redox cycle. *Energy Convers. Manag.* **2018**, *168*, 421–453. [CrossRef]
20. Bulfin, B.; Vieten, J.; Agrafiotis, C.; Roeb, M.; Sattler, C. Applications and limitations of two step metal oxide thermochemical redox cycles; A review. *J. Mater. Chem. A* **2017**, *5*, 18951–18966. [CrossRef]
21. Alonso, E.; Pérez-Rábago, C.; Licurgo, J.; Fuentealba, E.; Estrada, C.A. First experimental studies of solar redox reactions of copper oxides for thermochemical energy storage. *Sol. Energy* **2015**, *115*, 297–305. [CrossRef]
22. Haseli, P.; Jafarian, M.; Nathan, G.J. High temperature solar thermochemical process for production of stored energy and oxygen based on CuO/Cu_2O redox reactions. *Sol. Energy* **2017**, *153*, 1–10. [CrossRef]
23. Hänchen, M.; Stiel, A.; Jovanovic, Z.R.; Steinfeld, A. Thermally driven copper oxide redox cycle for the separation of oxygen from gases. *Ind. Eng. Chem. Res.* **2012**, *51*, 7013–7021. [CrossRef]
24. Clayton, C.K.; Whitty, K.J. Measurement and modeling of decomposition kinetics for copper oxide-based chemical looping with oxygen uncoupling. *Appl. Energy* **2014**, *116*, 416–423. [CrossRef]
25. Alonso, E.; Pérez-Rábago, C.; Licurgo, J.; Gallo, A.; Fuentealba, E.; Estrada, C.A. Experimental aspects of CuO reduction in solar-driven reactors: Comparative performance of a rotary kiln and a packed-bed. *Renew. Energy* **2017**, *105*, 665–673. [CrossRef]
26. Schrader, A.J.; Muroyama, A.P.; Loutzenhiser, P.G. Solar electricity via an Air Brayton cycle with an integrated two-step thermochemical cycle for heat storage based on Co_3O_4/CoO redox reactions: Thermodynamic analysis. *Sol. Energy* **2015**, *118*, 485–495. [CrossRef]
27. Block, T.; Knoblauch, N.; Schmücker, M. The cobalt-oxide/iron-oxide binary system for use as high temperature thermochemical energy storage material. *Thermochim. Acta* **2014**, *577*, 25–32. [CrossRef]
28. Agrafiotis, C.; Roeb, M.; Schmücker, M.; Sattler, C. Exploitation of thermochemical cycles based on solid oxide redox systems for thermochemical storage of solar heat. Part 2: Redox oxide-coated porous ceramic structures as integrated thermochemical reactors/heat exchangers. *Sol. Energy* **2015**, *114*, 440–458. [CrossRef]
29. Neises, M.; Tescari, S.; de Oliveira, L.; Roeb, M.; Sattler, C.; Wong, B. Solar-heated rotary kiln for thermochemical energy storage. *Sol. Energy* **2012**, *86*, 3040–3048. [CrossRef]

30. Tescari, S.; Agrafiotis, C.; Breuer, S.; De Oliveira, L.; Neises-Von Puttkamer, M.; Roeb, M.; Sattler, C. Thermochemical solar energy storage via redox oxides: Materials and reactor/heat exchanger concepts. *Energy Procedia* **2013**, *49*, 1034–1043. [CrossRef]
31. Singh, A.; Tescari, S.; Lantin, G.; Agrafiotis, C.; Roeb, M.; Sattler, C. Solar thermochemical heat storage via the Co_3O_4/CoO looping cycle: Storage reactor modelling and experimental validation. *Sol. Energy* **2017**, *144*, 453–465. [CrossRef]
32. Karagiannakis, G.; Pagkoura, C.; Halevas, E.; Baltzopoulou, P.; Konstandopoulos, A.G. Cobalt/cobaltous oxide based honeycombs for thermochemical heat storage in future concentrated solar power installations: Multi-cyclic assessment and semi-quantitative heat effects estimations. *Sol. Energy* **2016**, *133*, 394–407. [CrossRef]
33. Pagkoura, C.; Karagiannakis, G.; Zygogianni, A.; Lorentzou, S.; Kostoglou, M.; Konstandopoulos, A.G.; Rattenburry, M.; Woodhead, J.W. Cobalt oxide based structured bodies as redox thermochemical heat storage medium for future CSP plants. *Sol. Energy* **2014**, *108*, 146–163. [CrossRef]
34. André, L.; Abanades, S. Investigation of metal oxides, mixed oxides, perovskites and alkaline earth carbonates/hydroxides as suitable candidate materials for high-temperature thermochemical energy storage using reversible solid-gas reactions. *Mater. Today Energy* **2018**, *10*, 48–61. [CrossRef]
35. André, L.; Abanades, S.; Cassayre, L. High-temperature thermochemical energy storage based on redox reactions using Co-Fe and Mn-Fe mixed metal oxides. *J. Solid State Chem.* **2017**, *253*, 6–14. [CrossRef]
36. André, L.; Abanades, S.; Cassayre, L. Experimental Investigation of Co–Cu, Mn–Co, and Mn–Cu Redox Materials Applied to Solar Thermochemical Energy Storage. *ACS Appl. Energy Mater.* **2018**, *1*, 3385–3395. [CrossRef]
37. Carrillo, A.J.; Serrano, D.P.; Pizarro, P.; Coronado, J.M. Improving the Thermochemical Energy Storage Performance of the Mn_2O_3/Mn_3O_4 Redox Couple by the Incorporation of Iron. *ChemSusChem* **2015**, *8*, 1947–1954. [CrossRef] [PubMed]
38. Karagiannakis, G.; Pagkoura, C.; Zygogianni, A.; Lorentzou, S.; Konstandopoulos, A.G. Monolithic ceramic redox materials for thermochemical heat storage applications in CSP plants. *Energy Procedia* **2013**, *49*, 820–829. [CrossRef]
39. Carrillo, A.J.; Serrano, D.P.; Pizarro, P.; Coronado, J.M. Thermochemical heat storage based on the Mn_2O_3/Mn_3O_4 redox couple: Influence of the initial particle size on the morphological evolution. *J. Mater. Chem. A* **2014**, *2*, 19435–19443. [CrossRef]
40. Gillot, B.; El Guendouzi, M.; Laarj, M. Particle size effects on the oxidation-reduction behavior of Mn_3O_4 hausmannite. *Mater. Chem. Phys.* **2001**, *70*, 54–60. [CrossRef]
41. Block, T.; Schmücker, M. Metal oxides for thermochemical energy storage: A comparison of several metal oxide systems. *Sol. Energy* **2016**, *126*, 195–207. [CrossRef]
42. Monazam, E.R.; Breault, R.W.; Siriwardane, R. Kinetics of magnetite (Fe_3O_4) oxidation to hematite (Fe_2O_3) in air for chemical looping combustion. *Ind. Eng. Chem. Res.* **2014**, *53*, 13320–13328. [CrossRef]
43. Kozuka, H. *Handbook of Sol-Gel Science and Technology*; Volume 1: Sol-gel Processing; Sakka, S., Ed.; Springer Science & Business Media: Berlin, Germany, 2005; 680 p.
44. Carrillo, A.J.; Serrano, D.P.; Pizarro, P.; Coronado, J.M. Understanding Redox Kinetics of Iron-Doped Manganese Oxides for High Temperature Thermochemical Energy Storage. *J. Phys. Chem. C* **2016**, *120*, 27800–27812. [CrossRef]
45. Carrillo, A.J.; Moya, J.; Bayón, A.; Jana, P.; De La Peña O'Shea, V.A.; Romero, M.; Gonzalez-Aguilar, J.; Serrano, D.P.; Pizarro, P.; Coronado, J.M. Thermochemical energy storage at high temperature via redox cycles of Mn and Co oxides: Pure oxides versus mixed ones. *Sol. Energy Mater. Sol. Cells* **2014**, *123*, 47–57. [CrossRef]
46. Motuzas, J.; Diniz Da Costa, J.C. Copper aided exchange in high performance oxygen production by CuCo binary oxides for clean energy delivery. *J. Mater. Chem. A* **2015**, *3*, 17344–17350. [CrossRef]
47. Kang, Y.B.; Jung, I.H. Thermodynamic modeling of oxide phases in the Fe–Mn–O system. *J. Phys. Chem. Solids* **2016**, *98*, 237–246. [CrossRef]
48. Adánez-Rubio, I.; Izquierdo, M.T.; Abad, A.; Gayán, P.; de Diego, L.F.; Adánez, J. Spray granulated Cu-Mn oxygen carrier for chemical looping with oxygen uncoupling (CLOU) process. *Int. J. Greenh. Gas Control* **2017**, *65*, 76–85. [CrossRef]

49. Golikov, Y.V.; Tubin, S.Y.; Barkhatov, V.P.; Balakirev, V.F. Phase Diagrams of the Co-Mn-O System in Air. *J. Phys. Chem. Solids* **1985**, *46*, 539–544. [CrossRef]
50. Driessens, F.C.M.; Rieck, G.D. Phase Equilibria in the System Cu-Mn-O. *Z. Anorg. Allg. Chem.* **1967**, *351*, 48–62. [CrossRef]
51. Wei, P.; Bieringer, M.; Cranswck, L.M.D.; Petric, A. In-situ High Temperature X-ray and Neutron Diffraction of Cu-Mn Oxide Phases. *J. Mater. Sci.* **2010**, *45*, 1056–1064. [CrossRef]
52. Shishin, D.; Hidayat, T.; Jak, E.; Decterov, S.A. Critical assessment and thermodynamic modeling of the Cu–Fe–O system. *Calphad* **2013**, *41*, 160–179. [CrossRef]
53. Jacob, K.T.; Fitzner, K.; Alcock, C.B. Activities in the spinel solid solution, phase equilibria and thermodynamic properties of ternary phases in the system Cu-Fe-O. *Met. Trans. B* **1977**, *8*, 451–460. [CrossRef]
54. Zhang, W.-W.; Chen, M. Thermodynamic Modeling of the Co-Fe-O System. *Calphad* **2013**, *41*, 76–88. [CrossRef]
55. Jung, I.-H.; Decterov, S.A.; Pelton, A.D.; Kim, H.-M.; Kang, Y.-B. Thermodynamic Evaluation and Modeling of the Fe-Co-O System. *Acta Mater.* **2004**, *52*, 507–519. [CrossRef]
56. Zabdyr, L.A.; Fabrichnaya, O.B. Phase Equilibria in the Cobalt Oxide-Copper Oxide System. *J. Phase Equilib.* **2002**, *23*, 149–155. [CrossRef]
57. Crum, J.V.; Riley, B.J.; Vienna, J.D. Binary Phase Diagram of the Manganese Oxide-Iron Oxide System. *J. Am. Ceram. Soc.* **2009**, *92*, 2378–2384. [CrossRef]
58. Kjellqvist, L.; Selleby, M. Thermodynamic assessment of the Cr-Mn-O system. *J. Alloys Coump.* **2010**, *507*, 84–92. [CrossRef]
59. Bale, C.W.; Bélisle, E.; Chartrand, P.; Decterov, S.A.; Eriksson, G.; Gheribi, A.E.; Hack, K.; Jung, I.H.; Kang, Y.B.; Melançon, J.; et al. FactSage Thermochemical Software and Databases, 2010–2016. *Calphad* **2016**, *54*, 35–53. [CrossRef]
60. Carrillo, A.J.; Serrano, D.P.; Pizarro, P.; Coronado, J.M. Manganese oxide-based thermochemical energy storage: Modulating temperatures of redox cycles by Fe-Cu co-doping. *J. Energy Storage* **2016**, *5*, 169–176. [CrossRef]
61. Pashkova, E.V.; Novosadvoa, E.B.; Chalyi, V.P.; Antishko, A.N. Phase Diagram of the Manganese, Iron, and Cobalt oxides. *Ukr. Chem. J.* **1987**, *53*, 26–29.
62. Lalanne, M.; Barnabé, A.; Mathieu, F.; Tailhades, P. Synthesis and Thermostructural Studies of a $CuFe_{1-x}Cr_xO_2$ Delafossite Solid Solution with $0 \leq x \leq 1$. *Inorg. Chem.* **2009**, *48*, 6065–6071. [CrossRef] [PubMed]